Thermochimica Acta 512 (2011) 134–141

Contents lists available at ScienceDirect

Thermochimica Acta

journal homepage: www.elsevier.com/locate/tca

Sintering kinetics study of mechanically alloyed nanocrystalline Mo–30 wt.% W

Bhaskar Paul[a,*], Dheeraj Jain[b], S.P. Chakraborty[a], I.G. Sharma[a], C.G.S. Pillai[b], A.K. Suri[a]

[a] Materials Group, Bhabha Atomic Research Centre, Mumbai 400 085, India
[b] Chemistry Division, Bhabha Atomic Research Centre, Mumbai 400 085, India

ARTICLE INFO

Article history:
Received 13 April 2010
Received in revised form
15 September 2010
Accepted 16 September 2010
Available online 22 September 2010

Keywords:
Sintering
Activation energy
TMA
Kinetics
Nanocrystalline

ABSTRACT

The paper details the results of sintering kinetics studies conducted on nanocrystalline Mo–30 wt.% W alloy powders prepared through mechanical alloying route. Both, constant rate of heating method as well as Stepwise Isothermal Dilatometry (SID) technique were used for studying the sintering kinetics. Measured step isothermal shrinkage data were analyzed by Mekipritti-Meng method. The shrinkage data was found to fit well with the rate equation proposed in this method and its validity was established for mechanically alloyed systems. Kinetic parameters were evaluated and sintering was found to occur through two major mechanisms operative successively, which are grain boundary diffusion and lattice diffusion with corresponding energies of activation as 230 kJ/mol and 480 kJ/mol, respectively. The results have been well supported by micro structural evaluation of specimens at different stages of sintering.

1. Introduction

Mo–30 wt.% W alloy is of interest as a high temperature nuclear structural material because of its better formability, high temperature strength and improved oxidation resistance as compared to other Mo based alloys [1,2]. It is extensively used as components for Zinc processing, e.g. pump components, nozzles, thermocouple sheaths, stirrers for the glass industry, sputter targets for coating technology, etc. Preparation of Mo–30 wt.% W alloy by the conventional melt-casting process is a highly energy intensive process. The reasons can be attributed to the following facts. Firstly, very high melting points (2893 K and 3653 K for Mo and W, respectively) and a large difference in the specific gravity (10.2 g/cc and 19.32 g/cc for Mo and W, respectively) of the alloying components results in a number of melting runs required for thorough homogenization at very high temperatures nearly 3300 K. Secondly, a very high level of vacuum has to be maintained during melting as the alloying components can be oxidized even with the trace amount of air present in the reaction vessel. On the other hand, mechanical alloying has emerged as an alternative route in the recent past that has drawn wide attention for preparation of advance materials after its discovery by Schwarz and Koch [3]. Preparation of alloys through this route not only provides microstructural refinement but also imparts very high homogeneity of the final product [4,5]. Apart from this, a significantly less energy requirement for the alloy preparation, as compared to the conventional melt-casting technique makes this method economically attractive.

Once a homogeneous alloy powder is prepared, the next important task is to convert it into desired shapes with appropriate mechanical and physical properties. Sintering of these powders therefore becomes utmost important during shaping. Most of the molybdenum based products are produced by adopting powder metallurgical processing sequences including pressing and sintering followed by mechanical working in order to achieve near theoretical density and desired microstructure of the final product. Understanding the sintering mechanism of these powders therefore becomes very essential from both applied as well as research point of view. In this regard, a prior knowledge of the initial stage of sintering is very important to understand its exact mechanism. Considerable efforts have been made in the past to understand the kinetics and mechanisms involved during the initial stage of sintering [6–8]. Few studies on sintering of molybdenum [9–12] and tungsten [13–15] have also been reported earlier. Gospodinov et al. [16] studied the activated sintering of a mixture of tungsten and molybdenum powders in presence of Ni. However, to the best of our knowledge, the details of exact sintering kinetics of Mo–W alloy powder are not available in the open literature.

In the present study, we have attempted to evaluate the kinetics of sintering from both, the non-isothermal, i.e. constant rate of heating (CRH) method as well as the Stepwise Isothermal Dilatometry method. Model sintering equations suggested by Young and Cutler [17], originally developed by Johnson and coworkers [18] were used to analyze the shrinkage data generated during non-isothermal constant rate of heating (CRH) schedule.

* Corresponding author. Tel.: +91 22 25590183; fax: +91 22 25505151/19613.
E-mail addresses: bpaul@barc.gov.in, er_bhaskar2001@yahoo.com (B. Paul).

0040-6031/$ – see front matter © 2010 Elsevier B.V. All rights reserved.
doi:10.1016/j.tca.2010.09.015

Stepwise Isothermal Dilatometry (SID) is a relatively new approach as compared to conventional sintering studies and has proven its usefulness in analyzing the sintering mechanism of fine ceramic powders [19–22]. In our earlier work [23], we have shown the utility of this approach for studying the sintering kinetics of submicron sized Co metal powders. With this approach, it is possible to evaluate both, the sintering mechanism and the apparent activation energies using a single shrinkage data obtained from dilatometry. The same approach has been used to determine the possible mechanism of sintering in the present work. Observed results from SID have been analyzed by a model given by Makipirtti-Meng [19–23]. It has been found that the model fits equally well to explain the sintering kinetics of alloys systems prepared through mechanical alloying. Using kinetic data on densification, the diffusion coefficients for different mass transport mechanisms have been evaluated. Evolution of microstructure during the course of sintering has been studied in detail by SEM.

2. Theory

2.1. Sintering kinetics using constant rate of heating (CRH) method

Johnson [18] suggested the basic sintering equations individually for volume and grain boundary diffusion as

$$y_{Vol}^2 = \left(\frac{5.26\gamma\Omega D_V t}{kTa^3}\right) \tag{1}$$

$$y_{gb}^3 = \left(\frac{2.63\gamma\Omega b D_B t}{kTa^4}\right) \tag{2}$$

where y is the net linear shrinkage ($\Delta l/l_o$); Ω, the volume of vacancy (m^3); γ, the surface energy (J/m^2); D_V, the volume diffusion coefficient given by $D_V = D_V^0 \exp(-Q_V/RT)$ (m^2/s); bD_B, the product of grain boundary thickness 'b' and grain boundary diffusion coefficient 'D_B' given by $bD_B = bD_B^0 \exp(-Q_{bD_B}/RT)$ (m^3/s); k, the Boltzmann constant (J/K); T, the temperature (K); a, the particle radius (m) and t is time (s), Q_V and Q_{bD_B} are the activation energy for volume diffusion and grain boundary diffusion, respectively.

Sintering kinetics utilizing the constant rate of heating ('CRH', i.e. $c = T/t = dT/dt$) technique for the initial stage of densification (~5%), using different models has been reported by different researchers. For submicron size powder systems, sintering begins even before the steady state of isothermal part is reached. To account for that, sintering has been studied by CRH method. Above equations, originally suggested by Johnson have undergone further modification by different research groups. Out of the several modifications, the one proposed by Young and Cutler [17] however, is mostly used. The modified equations individually developed for volume and grain boundary diffusion, as suggested by them are given as Eqs. (3) and (4), respectively.

$$\ln\left(yT\ \frac{dy}{dT}\right) = \ln\left(\frac{2.63\gamma\Omega D_V^0}{ka^3c}\right) - \left(\frac{Q_V}{RT}\right) \tag{3}$$

$$\ln\left(y^2T\ \frac{dy}{dT}\right) = \ln\left(\frac{0.71\gamma\Omega bD_B^0}{ka^4c}\right) - \left(\frac{Q_{bD_B}}{RT}\right) \tag{4}$$

From above equations, it is clear that the activation energies for volume diffusion and grain boundary diffusion are obtained from the slopes of the plots between $\ln(yT\,dy/dT)$ versus $1/T$ and $\ln(y^2T\,dy/dT)$ versus $1/T$, respectively.

2.2. Sintering kinetics using Stepwise Isothermal Dilatometry (SID)

Rate-controlled sintering (RCS) of green compacts has been developed and studied widely for optimized densification and grain size control [24,25]. The prime feature of RCS is the control of the sintering process according to a specific shrinkage rate profile. It aims to eliminate the pores in an efficient way by controlling the diffusion kinetics of the material. Similar to this, Stepwise Isothermal Dilatometry (SID) is one more approach to understand sintering kinetics. Makipirtti and Meng [19–23] proposed a model to analyze the SID shrinkage data. According to this model, the fractional densification function Y, for an isotropic sintering behavior is expressed as

$$Y = \frac{V_O - V_t}{V_O - V_f} = \frac{L_O^3 - L_t^3}{L_O^3 - L_f^3} \tag{5}$$

where V_O (L_O), V_t (L_t), and V_f (L_f) are the initial volume (length), volume (length) at time t, and volume (length) of the finally densified specimen, respectively. A normalized rate equation as suggested by Makipirtti-Meng method is given as

$$\frac{dY}{dt} = nk(T)Y(1-Y)\left(\frac{1-Y}{Y}\right)^{1/n} \tag{6}$$

$$k(T) = k_o\ \exp\left(\frac{-Q}{RT}\right) \tag{7}$$

where $k(T)$ is specific rate constant, k_o, the frequency factor, Q, the energy of activation, R, the universal gas constant and n is a parameter related to the sintering mechanism.

3. Experimental

3.1. Preparation and characterization of nanocrystalline Mo–30 wt.% W alloy powder

Elemental powders of Mo and W with a purity of 99.9% and an average agglomerate size of 5 and 6 μm, respectively were mixed in the desired composition ratio of Mo–30 wt.% W and subjected to mechanical alloying in a high energy planetary ball mill for different durations from 5 h to a maximum of 25 h. The as milled powders were characterized for their phase and chemical composition by room temperature powder XRD and EDX analysis, respectively. X-ray diffraction pattern of the powders were recorded on a powder diffractometer (model-PW 1820, Philips) with Ni filtered Cu Kα radiation, operating at 30 kV and 20 mA. All diffraction patterns were recorded in the 2θ range from 35 to 50°, with a slow scanning rate of step size 0.002°/s. The crystallite size of these powders was determined using X-ray line broadening of (1 1 0) peak of the alloy and calculated using the Scherrer equation [26]. Si single crystal was used as an external standard for calibration as well as deduction of instrumental broadening.

$$\tau = \frac{0.9\lambda}{\beta\ \cos\theta} \tag{8}$$

$$\beta^2 = \beta_m^2 - \beta_s^2 \tag{9}$$

where τ is the average diameter of the crystallites in Å. β_m, β_s are the measured width at half the maximum intensity (FWHM) of the (1 1 0) reflection line from the sample and 28.45° line of the Si standard, respectively, θ is the diffraction angle corresponding to the peak maximum, and λ is the Cu Kα weighted wavelength (λ = 1.5406 Å).

The as-milled powders were subsequently cold pressed into green compacts of 6 mm diameter and 5–6 mm length at a pressure of 300 MPa. Green densities of the samples were measured

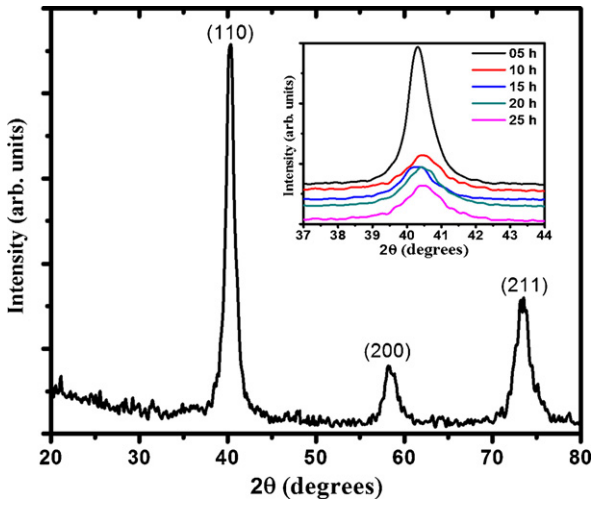

Fig. 1. XRD pattern of Mo–30 wt.% W powder prepared by mechanical alloying for 15 h. Inset shows the Mo (1 1 0) peak variation as a function of milling duration.

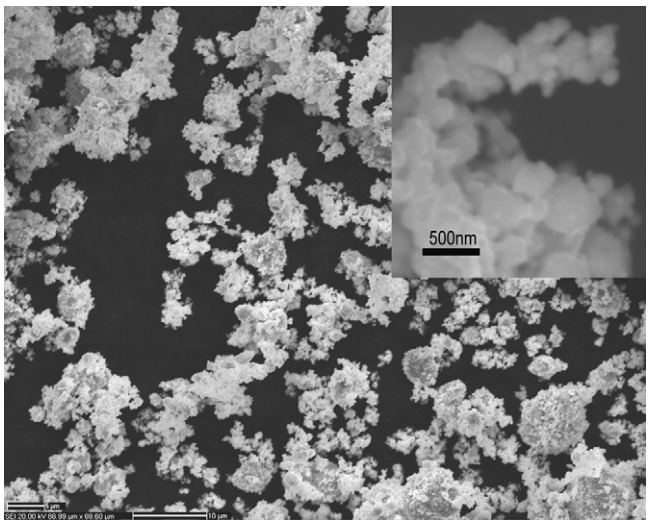

Fig. 2. SEM image of Mo–30 wt.% W powder prepared through mechanical alloying (25 h milling). Inset shows the higher magnification image of agglomerated particles to show the sub-micron nature of the powder.

using the geometrical dimensions. The morphology of the as-milled powders was observed with a scanning electron microscope (Model MV2300CT/100, Camscan, UK).

3.2. Sintering studies on Mo–30 wt.% W alloy powder

The green compacts were subjected to dilatometry to measure the changes in sample length during sintering for different heating schedules. All dilatometric measurements were carried out in a vertical type thermo mechanical analyzer (TMA) (Setsys Evolution TMA 1600, M/s SETARAM, France) with a minimum load (1 g) condition in reducing atmosphere (Ar–4% H_2, 20 ml/min). Shrinkage profiles were recorded by heating the green compacts at a heating rate of 20 K/min up to the programmed temperature followed by cooling (30 K/min) to ambient. One sample, already sintered up to 1573 K with an isothermal hold period of 1 h at the maximum temperature (under the same reducing conditions) was measured for its expansion behavior separately up to the same temperature with the same heating cycle in order to evaluate the linear thermal expansion behavior of this alloy. This expansion was subtracted from the as-measured shrinkage data of green compacts to determine the net shrinkage. A special sintering schedule was employed for recording the shrinkage behavior using Stepwise Isothermal Dilatometry (SID) method. In this experiment, shrinkage was continuously measured while heating the green pellet from 298 K to 973 K at a heating rate of 20 K/min and then onwards up to 1523 K with the same rate of heating and an isothermal hold of 30 min at each 50 K interval (step). The program was chosen in a manner so that shrinkage during the non-isothermal part can be minimized as far as possible. Densities of the sintered samples were measured both dimensionally as well as by Archimedes principle using water as the immersion liquid. Microstructures of samples sintered at different temperatures were studied using scanning electron microscopy.

4. Results and discussion

4.1. Phase analysis and powder morphology

Fig. 1 shows the room temperature X-ray diffraction pattern of the Mo–30 wt.% W powder prepared by mechanical alloying for 15 h. The alloyed powder has been found to have the single phase cubic molybdenum structure as revealed by a perfect match with the literature data (PCPDF-421120). The inset in Fig. 1 shows the enlarged view of the diffraction patterns corresponding to the principal (1 1 0) peak for powders prepared with different milling duration. Gradual peak broadening and decreasing peak intensity can be clearly observed with increasing milling time. This can be attributed to (a) decreasing crystallite size from 12.5 nm for 5 h milled powder to around after 5 h milling to about 7.6 nm for 25 h milled powder as revealed by crystallite size evaluation using peak broadening and (b) due to gradually increasing strain in the system with increasing milling time. Fig. 2 shows the SEM image of Mo–30 wt.% W powder prepared by mechanical alloying for 25 h, which reveals an agglomerated form of the powder. The average agglomerate size as measured from the SEM images is 15 (±3) μm. This agglomeration is mainly due to very small crystallites with very high surface energy being formed during mechanical alloying. This is further evident from the inset of Fig. 2, which clearly reveals the nanocrystalline nature of the as-prepared powder. Fig. 3 shows the EDX spectra of the same powder confirming the targeted chemical composition without any notable contamination during the alloying process. Fig. 4 presents the X-ray diffraction patterns corresponding to the principal (1 1 0) peak for as-compressed green pellet and pellets sintered to different temperatures. A shift of this reflection peak towards higher angles (from 40.32° for powder milled for 5 h to 40.58° for sintered at 1100 °C) is observed. This indicates a reduction in the lattice parameter of the sintered alloy and can be attributed to the (a) atomic radius mismatch between Mo and W and (b) distortion of the molybdenum lattice due to tungsten diffusion in it. A similar result of lattice distortion of Mo

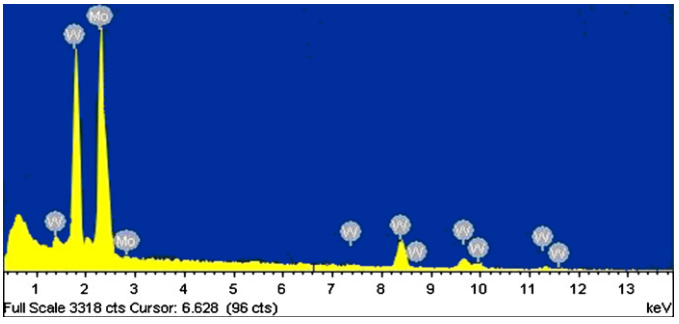

Fig. 3. EDX Spectra of as prepared Mo–30 wt.% W powder.

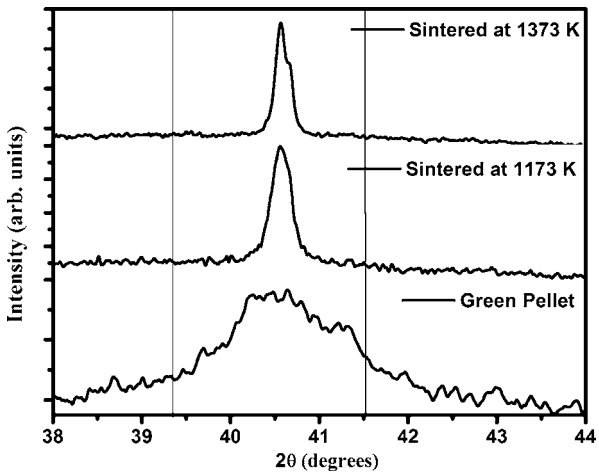

Fig. 4. XRD patterns of Mo (1 1 0) peak for (a) Mo–30 wt.% W green compact, (b) sample sintered up to 1173 K and (c) sample sintered up to 1373 K.

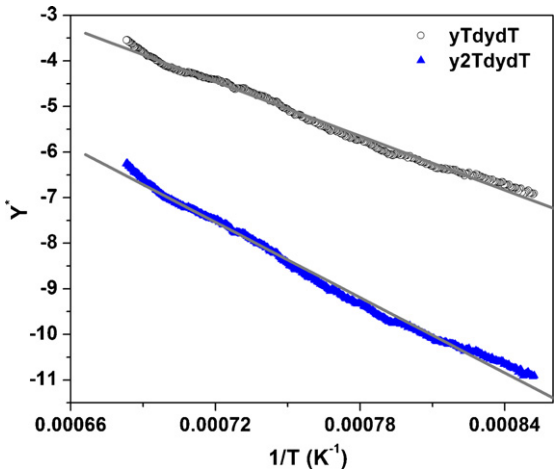

Fig. 6. Plot of $\ln(yT\,dy/dT)$ and $\ln(y^2T\,dy/dT)$ versus $1/T$. Grey line curve shows the least-squares linear fit of the evaluated data.

is reported by Gospodinov et al. for Mo–W system [16] due to the formation of W–Mo solid solution.

4.2. Sintering kinetics through nonisothermal shrinkage data

Fig. 5 shows the linear shrinkage profiles of Mo–30 wt.% W alloy powder compacts sintered at different temperatures with constant rate of heating schedule (CRH) keeping the rate of heating to be 20 K/min. It can be seen that the maximum shrinkage is achieved for sample heated up to 1573 K yielding nearly 91% (sintered density ~10.9 g/cc) theoretical density of Mo–30 wt.% W alloy. It can be visibly seen that instead of an initial expansion, normally expected due to usual thermal expansion of any material before the actual sintering commences, a small amount of shrinkage was observed while sintering these compacts under reducing atmosphere. The initial shrinkage observed at temperatures below 1023 K before the onset of actual sintering can be explained as due to (i) reduction of surface contamination (oxides) layers to metal and thus reducing the volume and (ii) very high surface energy and highly deformed nature of the sub-micron sized powders that facilitate their aggregation at relatively lower temperatures and hence exhibiting shrinkage. This phenomenon has been illustrated in detail in one of our previous study [23]. Since the individual curves represent the shrinkage obtained at the same heating rate (20 K/min), ideally all these

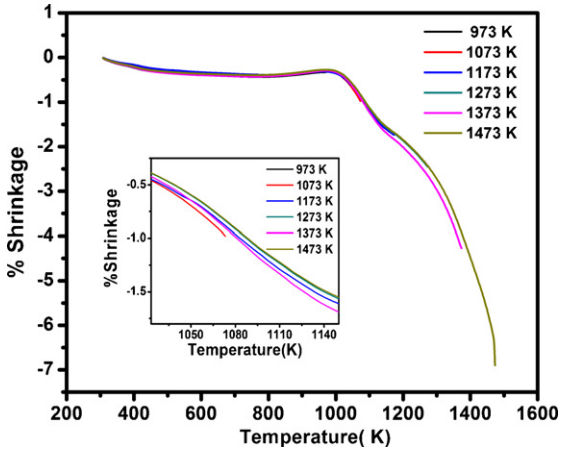

Fig. 5. Shrinkage profiles of Mo–30 wt.% W alloy powder compacts sintered at different temperatures with constant rate of heating (20 K/min). Inset shows the variation in shrinkage profile in different experiment.

should represent a single curve. Therefore an average of all the shrinkage values at given temperatures was obtained and was used for subsequent analysis. Further, as the model equations applicable to the initial stage of sintering were used for analysis of sintering kinetics, the shrinkage data was limited to 1473 K (i.e. up to ~5% of shrinkage). As explained earlier in Section 2.1, the plots of $\ln(yT\,dy/dT)$ versus $1/T$ and $\ln(y^2T\,dy/dT)$ versus $1/T$, that are shown in Fig. 6 together, allow the calculation of activation energy and the frequency factor for volume diffusion and grain boundary diffusion, respectively as presented in Table 1.

The similarity in the two Arrhenius plots shown in Fig. 6 suggests that the mechanism for sintering here could be either volume diffusion or grain boundary diffusion or simultaneous occurrence of both [27]. Actually, the diffusion rate is determined by temperature, powder characteristics and the specific structure of material. Further, the diffusion rate determines the paths of diffusion, through the volume or the boundaries of crystals, dislocations, or the surfaces. Volume diffusion in crystals is the most difficult material transport mechanism with the highest activation energy barrier associated with it. The path then becomes easier for diffusion through dislocations, boundaries and surfaces [28]. However, in the present system, the calculated activation energy for volume diffusion (190 kJ/mol) seems to be erroneous (towards a lower side) since the reported activation energy value for pure Mo is much higher (~400 kJ/mol) [29]. Although Davade et al. [27] have also reported a lower activation energy for lattice diffusion than grain boundary diffusion, they substantiated the observation by the term called 'enhanced boundary diffusion'.

While it was initially thought that volume diffusion was the dominant sintering mechanism in the densification of pure molybdenum or Mo based alloys [12], studies on activated sintering showed [12,16] that the grain boundary mobility retarded the densification process, thus causing the apparent activation energy to be driven up to the values that appeared more in line with volume diffusion. The consensus among the researchers however is that grain boundary diffusion is considered to be the dominant densification mechanism for most of the Mo based alloys [30]. Our results also match with the same line of thought. Thus the model employed here does give an idea about the dominant mechanism

Table 1
Kinetic parameters for CRH sintering of Mo–30 wt.% W alloy.

Q_{GB} (kJ/mol)	Q_V (kJ/mol)	$bD_B{}^0$ (m^3/s)
230	190	7.44×10^{-9}

Table 2
Values of bD_B were calculated at various temperatures and are presented in Table 2.

Temperature (K)	bD_B (m^3/s)
973	3.1×10^{-21}
1023	1.3×10^{-20}
1073	4.5×10^{-20}
1123	1.4×10^{-19}

during the initial stage of sintering, which is grain boundary diffusion with an activation energy of ~230 kJ/mol. Using the expression $bD_B = bD_B^O\, e^{(-Q_{bD_B}/RT)}$, the values of bD_B were calculated at various temperatures and are presented in Table 2. The values fall well in line with the expected trend of increasing grain boundary diffusion coefficients with increasing temperatures.

4.3. Analysis of stepwise isothermal shrinkage data

Fig. 7 shows the shrinkage profile and shrinkage rate of the green compact subjected to SID sintering schedule. It also shows the variation of shrinkage rate occurring at each isothermal step during sintering. The experimental shrinkage curve obtained by dilatometery is generally in the form of [18,31]:

$$y = [k(T)t]^m \tag{10}$$

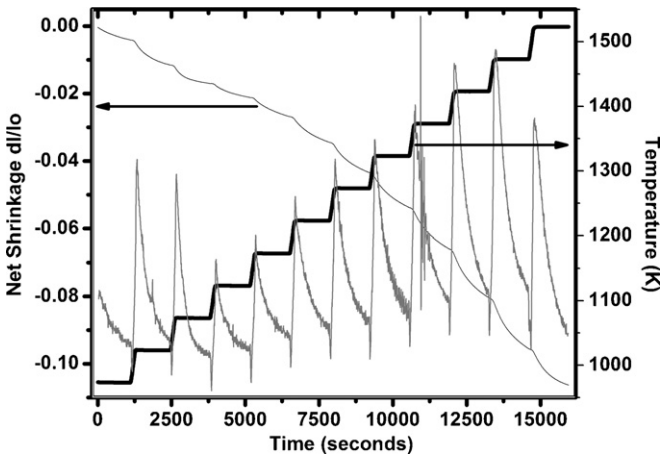

Fig. 7. SID shrinkage profile of Mo–30 wt.% W alloy green compact along with the temperature program followed for the SID experiment. The curve in grey color show the shrinkage rate $\{d(l/l_o)/dt\}$ as a function of time.

If volume diffusion is the only operative mechanism, then the shrinkage rate is given by

$$\frac{dy}{dt} = n\left(\frac{5.34\gamma\Omega D_V}{kTa^3}\right)^m t^{(m-1)} \tag{11}$$

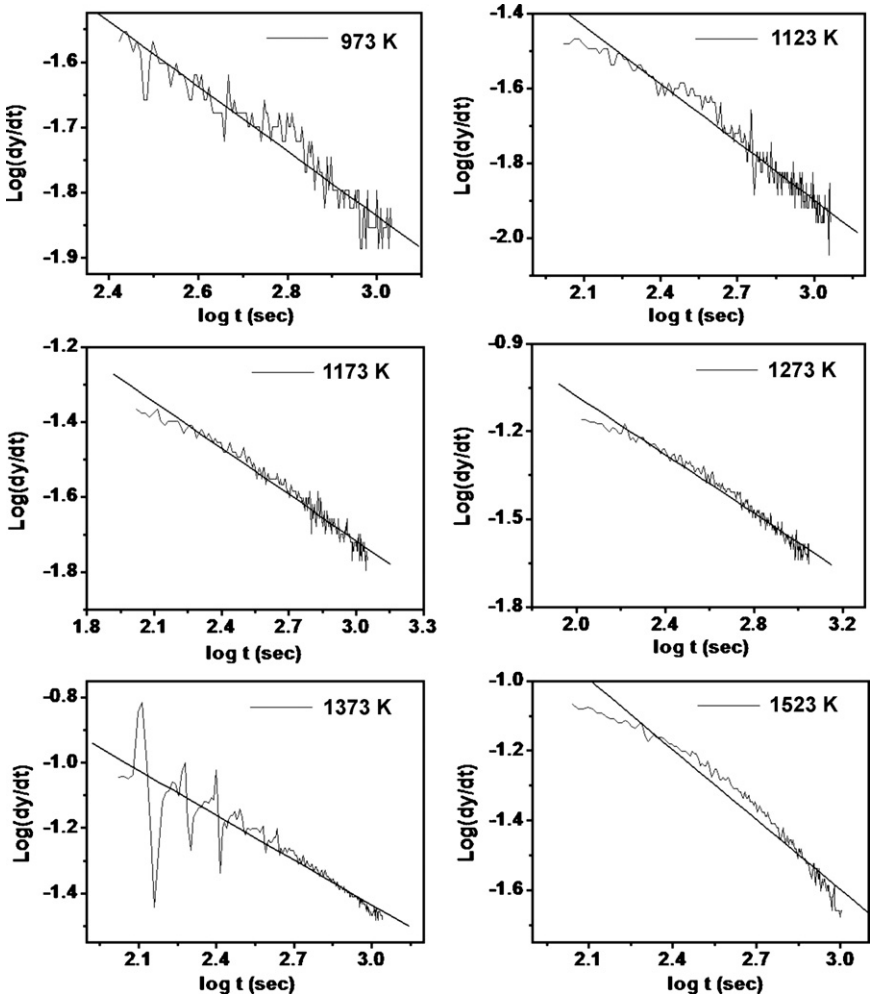

Fig. 8. Plot of $\log(dy/dt)$ vs. $\log t$ at different isothermal steps.

Table 3
Volume diffusion coefficients for Mo–30 wt.% W alloy evaluated through SID analysis.

Temperature (K)	D_V (m^2/s)
900	1.5×10^{-19}
1000	4.9×10^{-18}
1100	1.4×10^{-16}
1200	2.3×10^{-15}

Similarly, if the grain boundary diffusion is operative solely, then the shrinkage rate is given as

$$\frac{dy}{dt} = n\left(\frac{2.14\gamma\Omega bD_B}{kTa^4}\right)^m t^{(m-1)} \quad (12)$$

Fig. 8 shows the plot between log(dy/dt) and log t for different isothermal steps. From the slope of the plots, the sintering exponents 'm' has been determined for each isothermal step. The value of 'm' varies from ~(0.2 to 0.3) up to 1073 K to 0.5 up to 1473 K. It is therefore evident that for temperature up to 1073 K, grain boundary diffusion (GB) is the rate controlling mechanism. However, from the next step, volume diffusion takes over as the rate controlling mechanism of sintering. From the values of intercepts, the diffusion coefficients at different temperatures have been evaluated and presented in Table 3. The coefficients evaluated here are very close to the reported diffusion coefficients for pure molybdenum (1.6×10^{-15} m^2/s) and tungsten (1.3×10^{-15} m^2/s) at 1773 K evaluated by high temperature tracer determinations [32]. This is very close to the values obtained in this study.

Using Makipirtti-Meng model, as described earlier in Section 2.2, the shrinkage data, after fitting into Eq. (6) is plotted in Fig. 9 as $\ln\{(dY/dt)/Y/(1-Y)\}$ versus $\ln[(1-Y)/Y]$. A near straight line behavior for each isothermal zone indicates the validity of the model with present shrinkage data of Mo–30 wt.% W alloy. The Values of slope '$1/n$' and intercept '$\ln nk(T)$', evaluated by least-squares linear fitting for each straight line segment of the curve, are presented in Table 4. Parameter 'n', that relates to the sintering mechanism takes nearly two different average values in the measured temperature range as $1/n \sim 0.2$ (1373–1473 K) and ~0.13–0.18 (1073–1323 K). These values suggest that there are two different sintering mechanisms, operative as the dominant processes over the above temperature intervals. Fig. 10 shows the Arrhenius plot between $\ln k(T)$ and $1/T$ for the SID shrinkage data. The curve can be best fitted into two linear segments in the temperature ranges from 973 to 1173 K and 1173–1523 K. The apparent

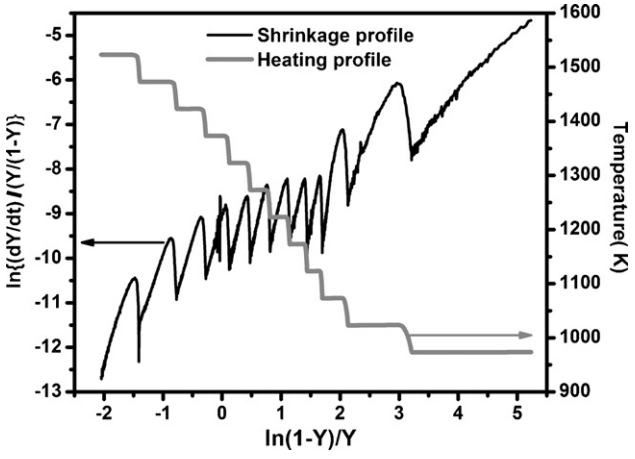

Fig. 9. Plots of $\ln\{(dY/dt)/Y/(1-Y)\}$ vs. $\ln\{(1-Y)/Y\}$ according to Mekipritti-Meng equation. Variation of temperature with time is also shown on the right hand scale.

Table 4
Kinetic analysis of SID shrinkage data of Mo–30 wt.% W alloy green compacts according to Makipritti-Meng equation.

Temperature (K)	$1/n$	n	$\ln k(T)$	Regression parameter
973	0.588	1.69	−20.20	0.994
1023	0.304	3.29	−19.37	0.995
1073	0.149	6.67	−17.23	0.994
1123	0.134	7.41	−16.12	0.991
1173	0.182	5.48	−15.84	0.992
1223	0.170	5.87	−14.48	0.988
1273	0.164	6.07	−12.82	0.992
1323	0.176	5.65	−10.85	0.991
1373	0.202	4.94	−9.05	0.994
1423	0.218	4.58	−7.29	0.996
1473	0.259	3.85	−6.07	0.993

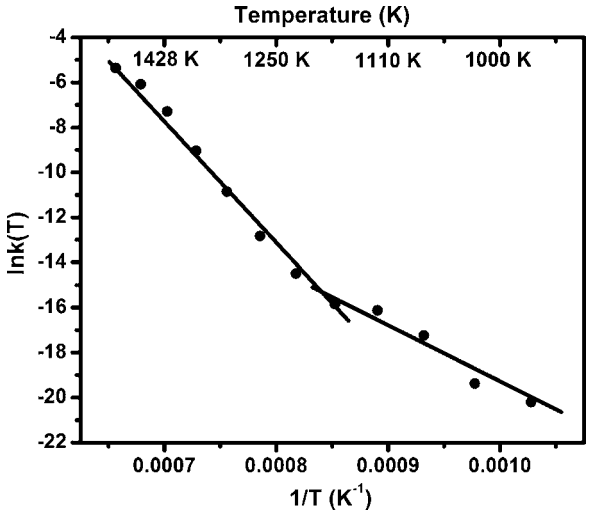

Fig. 10. Arrhenius plot of $\ln k(T)$ vs. $1/T$ based on the data in Table 4.

activation energy 'Q' was calculated from the slopes of each segment and compared with that of various sintering mechanisms reported in the literature [5,7]. The values are presented in Table 5. It is evident that the initial stage of sintering of Mo–30 wt.% W powder compacts can be divided into two main stages. The first stage (973–1173 K) relates to sintering within the aggregates, formed upon coalescence of the individual crystallites and leading to neck formation through grain boundary diffusion. This is further supported by the SEM image recorded on 1173 K sintered sample that shows initial stage of neck formation (Fig. 11(a)). The activation energy value calculated from the least square regression analysis of data between 973 and 1173 K comes out to be 230 kJ/mol. A higher value of activation energy (480 kJ/mol) for temperature range 1173–1523 K is an indicative of lattice diffusion as the dominant process for mass transport. The micrograph recorded on sample sintered at 1373 K (Fig. 11(c)) clearly reveals the same.

It is seen from the Fig. 7 that initially there is distinct shrinkage rate in the isothermal stage of 1023 and 1073 K and thereafter the shrinkage rate increases gradually with temperature. The maximum net shrinkage during an isothermal soak period occurs at

Table 5
Apparent activation energies evaluated from SID analysis.

Temperature range	Activation energy	Dominant mechanism
973–1173 K	230 kJ/mol	Grain boundary diffusion
1173–1523 K	480 kJ/mol	Lattice diffusion

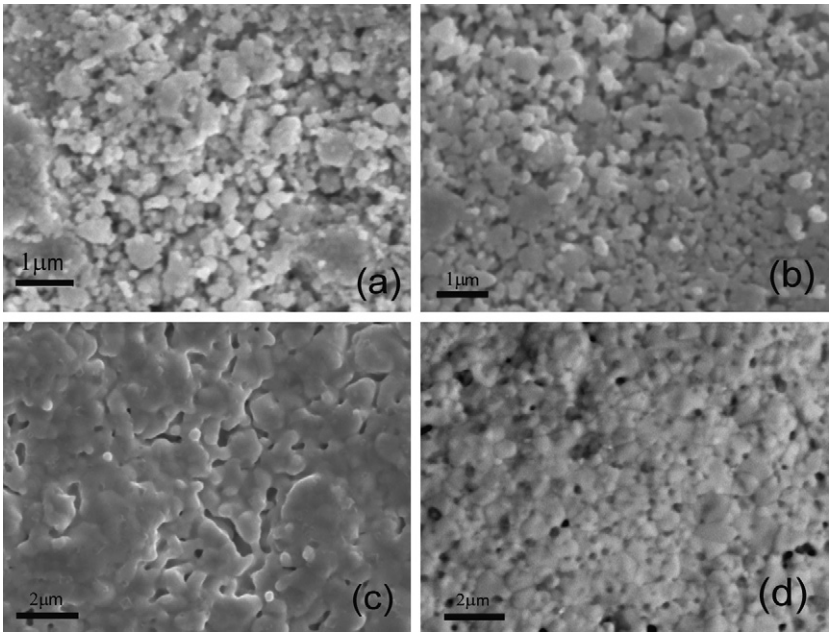

Fig. 11. SEM micrographs of Mo–30 wt.% W alloys sintered at temperatures: (a) 1173 K, (b) 1273 K, (c) 1373 K and (d) 1523 K.

1373 K with the maximum rate of shrinkage. The shrinkage rate then decreases with further temperature increase. The gradual increase in shrinkage rate with increasing temperature is due to enhanced thermally activated diffusion. The maxima in the shrinkage rate clearly accounts for all possible mass transport mechanisms operating in tandem. A further decrease in the rate of shrinkage is mainly due to grain growth related phenomena. With progressive grain growth, the effective area offered by the grain boundaries decreases in the system. Since the grain boundaries act as vacancy sink for mass transport from the bulk, a reduction in it lead to events that decrease the mass transport rate and hence a reduction in the observed shrinkage rate. Grain growth can occur only after a certain degree of shrinkage because the neck curvatures are initially very large and pin the grain boundaries [33]. In case of Mo–30 wt.% W, visible grain growth can be seen only beyond 1373 K as seen in the SEM image (Fig. 11(d)).

From the above discussion, it is therefore quite clear that the SID approach is a very useful tool to evaluate the sintering kinetics of metallic systems and gives fairly reliable values of the activation energies associated with different mechanism of mass transport using the dilatometry data of a single experiment. The model results are found to be consistent with the micro structural evaluation, as revealed by SEM analysis.

5. Conclusion

Sintering kinetics of sub micron sized Mo–30 wt.% W alloy powder prepared through mechanical alloying was studied by both, constant rate of heating (CRH) and Stepwise Isothermal Dilatometry (SID) technique. The observed experimental results demonstrated that the activation energy values calculated by SID method and CRH method are in good agreement. SID shrinkage data were analyzed by conventional and Mekipritti-Meng method to evaluate the sintering mechanism and activation energies. The Mekipritti-Meng model was found to fit well with the shrinkage data of Mo–30 wt.% W alloy powder and hence validated its usefulness for sintering studies of alloys. Sintering in this alloy occurs through two dominant mechanisms with average activation energies of 230 kJ/mol and 480 kJ/mol corresponding to grain boundary diffusion and lattice diffusion, respectively. The results are found to be consistent with the microstructural evaluation as studied by SEM analysis. Furthermore, the diffusivities calculated in this study agree well with previous reported values by high temperature tracer determinations.

Acknowledgements

The authors sincerely thank Dr. D. Das, Head, Chemistry Division, BARC and Dr. A.C. Bidaye, MPD, BARC for their constant encouragement and support during the course of this work.

References

[1] H.L. Brown, C.P. Kempter, J. Less-Comm. Met. 12 (1967) 166–168.
[2] D.-B. Lee, G. Simkovich, Oxid. Met. 31 (1989) 265–274.
[3] R.B. Schwarz, C.C. Koch, Appl. Phys. Lett. 49 (1986) 146–148.
[4] S. Cai, X. Ma, H. Tang, W. Zhao, J. Yan, B. Zhao, Z. Qiao, J. Alloys Compd. 430 (2007) 77–80.
[5] A. Bose, G. Jerman, R.M. German, Powder Metall. Int. 21 (1989) 9–13.
[6] W.D. Kingery, M. Berg, J. Appl. Phys. 26 (1955) 1205–1212.
[7] J.G.R. Rockland, Acta Metall. 14 (1966) 1273–1279.
[8] R.L. Coble, J. Am. Ceram. Soc. 41 (1958) 55–62.
[9] D.J. Jones, J. Less-Comm. Met. 2 (1960) 76–85.
[10] D.J. Sellers, M. Levy, J. Less-Comm. Met. 9 (1965) 289–298.
[11] R.M. German, Z.A. Munir, J. Less-Comm. Met. 58 (1978) 61–74.
[12] D.C. Blaine, J.D. Gurosik, S.J. Park, R.M. German, D.F. Heaney, Metall. Mater. Trans. A 37A (2006) 715–720.
[13] N.C. Kothari, J. Less-Comm. Met. 5 (1963) 140–150.
[14] J.A.M. Van Liempt, Rec. Trav. Chim 64 (1945) 239–245.
[15] X.F. Ashby, Acta Metall. 22 (1974) 275–289.
[16] G.A. Gospodinov, V.K. Pangarova, D.K. Lambiev, Sov. Powder Metall. Met. Ceram. 15 (1976) 159–161.
[17] W.S. Young, I.B. Cutler, J. Am. Ceram. Soc. 53 (1970) 659–663.
[18] D.L. Johnson, J. Appl. Phys. 40 (1969) 192–200.
[19] R. Yan, F. Chu, Q. Ma, X. Liu, G. Meng, Mater. Lett. 60 (2006) 3605–3609.
[20] G.Y. Meng, O.Toft. Sorensen, in: Y. Han (Ed.), Advanced Structural Materials, vol. 2, Elsevier Science Publishers B.V., Amsterdam, Netherlands, 1991, pp. 369–374.
[21] H.T. Wang, X.Q. Liu, F.L. Chen, G.Y. Meng, J. Am. Ceram. Soc. 81 (1998) 781–784.
[22] Y.F. Liu, X.Q. Liu, S.W. Tao, G.Y. Meng, O.Toft. Sorensen, Ceram. Int. 28 (2002) 479–486.
[23] B. Paul, D. Jain, A.C. Bidaye, I.G. Sharma, C.G.S. Pillai, Thermochim. Acta 488 (2009) 54–59.
[24] M.L. Huckabee, H. Palmour III, Am. Ceram. Soc. Bull. 51 (1972) 574–576.
[25] M. Kramer, J. Mater. Sci. Lett. 14 (1995) 778–782.

[26] B.D. Cullity, Elements of X-ray Diffraction, Addison-Welsey, Reading, MA, 1969.
[27] V.V. Dabhade, T.R. Rama Mohan, P. Ramakrishnan, Mater. Sci. Eng. A 452–453 (2007) 386–394.
[28] V.S. Bakunov, A.V. Belyakov, Glass Ceram. 50 (1993) 287–291.
[29] S. Majumdar, S. Raveendra, I. Samajdar, P. Bhargava, I.G. Sharma, Acta Mater. 57 (2009) 4158–4168.
[30] R.M. German, Sintering Theory and Practice, John Wiley and Sons, New York, 1996.
[31] D. Lahiri, S.V. Ramana Rao, G.V.S. Hemantha Rao, R.K. Srivastava, J. Nucl. Mater. 357 (2006) 88–96.
[32] D.F. Kalinovich, I.I. Kovenskii, M.D. Smolin, Sov. Powder Metall. Met. Ceram. 4 (1965) 324–326.
[33] P.E. Zovas, R.M. German, Metall. Mater. Trans. A 15 (1984) 1103–1109.